Finite volume effects in a quenched lattice-QCD quark propagator

C. S. Fischer and M. R. Pennington

IPPP, Durham University, Durham DH1 3LE, United Kingdom
(Received 20 December 2005; published 27 February 2006)

We investigate finite volume effects in the pattern of chiral symmetry breaking. To this end we employ a formulation of the Schwinger-Dyson equations on a torus which reproduces results from the corresponding lattice simulations of staggered quarks and from the overlap action. Studying the volume dependence of the quark propagator we find quantitative differences with the infinite volume result at small momenta and small quark masses. We estimate the minimal box length L below which chiral perturbation theory cannot be applied to be $L \simeq 1.6$ fm. In the infinite volume limit we find a chiral condensate of $|\langle \bar{q}q \rangle|_{\overline{MS}}^{2\,\text{GeV}} = (253 \pm 5 \text{ MeV})^3$, an up/down quark mass of $m_{\overline{MS}}^{2\,\text{GeV}} = 4.1 \pm 0.3$ MeV and a pion decay constant which is only 10% smaller than the experimental value.

I. INTRODUCTION

Dynamical chiral symmetry breaking is certainly one of the most interesting phenomena of QCD. It is entirely a strong coupling effect in the sense that dynamical quark masses cannot be generated at any order in perturbation theory. Thus nonperturbative methods like lattice Monte-Carlo simulations [1], chiral perturbation theory [2] or the Green's function approach using the Schwinger-Dyson and Bethe-Salpeter equations (SDE/BSE) [3,4], are needed to explore chiral symmetry and its breaking pattern.

With the rediscovery of the Ginsparg-Wilson relation and the construction of actions for overlap, domain wall and perfect fermions, the lattice formulation of QCD emerged in principle as an appropriate nonperturbative tool, with which to study the effects of dynamical chiral symmetry breaking. However, in practice, lattice simulations with small quark masses are extremely expensive in terms of CPU-time. It is only with staggered fermion actions that quark masses not far from their physical values have been achieved to date, but these actions have the disadvantage that full chiral symmetry is only recovered in the continuum limit. Consequently, there is no certainty with any finite volume that the correct breaking pattern can be observed.

Lattice simulations are, of course, always performed at a finite volume. Since continuous symmetries cannot be spontaneously broken at a finite volume V, chiral symmetry is restored in the limit of zero quark mass, $m \to 0$, independently of the formulation of the lattice action. Thus one first has to perform the limit $V \to \infty$ before one can investigate the chiral limit. At the hadron level, whether for mesons and baryons, chiral perturbation theory provides a reliable tool with which to make such an extrapolation (see e.g. [5–7] and references therein). Volume effects for any particles that couple to the pion can be arranged in powers of $\exp[-M_\pi L]$, where M_π is the pion mass and L is the size of the box [8]. On the other hand, chiral perturbation theory has nothing to say about volume effects in the

underlying quark and gluon substructure. For this the Green's function approach employing Schwinger-Dyson equations provides a suitable alternative. Indeed, a recent investigation of the gluon and ghost propagator of the Landau gauge Yang-Mills theory on a torus could offer an explanation for systematic differences in the infrared behavior of these propagators in a box, compared with the infinite volume limit [9].

In the present work we extend this analysis and investigate finite volume effects in the quark propagator. To this end we study the QCD-gap equation for the quark propagator on a torus. The input from the Yang-Mills sector of QCD consists of numerical solutions for the ghost and gluon propagator, which match corresponding lattice calculations [10,11]. Presently unknown contributions from the quark-gluon vertex are parametrised such that the quenched lattice quark propagators from each of Ref. [12] (staggered) and Ref. [13] (overlap) are reproduced by the gap equation. This idea has already been explored to some extent by Bhagwat *et al.* [14].

Our treatment differs from that of Ref. [14] in two essential respects: first, we solve the coupled set of three SDEs for the ghost, gluon and quark propagators, and so include the Yang-Mills sector of the SDEs in the Green's function approach. Second, we calculate our propagators on a manifold similar to that of the lattice and fit the interaction to reproduce the lattice results of the gluon and quark propagators on their respective manifolds.

One of the advantages of the Green's function approach is that volume effects can be studied continuously from very small to very large volumes (corresponding studies for meson observables using chiral perturbation theory e.g. have to distinguish between two different regions of chiral counting [7]). Furthermore, one has direct access to the infinite volume and the continuum limit without the need to perform any extrapolations. We are thus in a position to study chiral symmetry restoration at small volumes together with effects at large and infinite volumes in the same framework.

The paper is organized as follows: In the next section we shortly review basic properties of the pattern of dynamical chiral symmetry breaking in a box. In particular, we recall the derivation of the Casher-Banks relation and a basic estimate for a minimal box length for chiral perturbation theory. In Sec. III we discuss the technical details associated with solving the quark Schwinger-Dyson equation on a torus. Our results on the compact manifold are presented in Sec. IV. We start with a summary of finite volume effects in the Yang-Mills sector based on the results of Ref. [9]. These are used as input into the quark-SDE together with a model for the quark-gluon interaction, which is discussed in Sec. IV A. The interaction is fitted so that the lattice data for the quark propagator from Ref. [12] (staggered) and Ref. [13] (overlap), respectively, are reproduced by the quark-SDE. We then determine the corresponding quark propagator at larger volumes and in the infinite volume limit. The results are compared in Sec. IV B. For small quark masses we find sizeable quantitative volume effects which are still present at comparably large volumes. These effects are qualitatively similar for both the propagators from staggered and overlap quarks. The small volume behavior of the quark propagator is investigated in Sec. IV C. For a fixed, small current quark mass we determine the onset of dynamical chiral symmetry breaking when the volume of the box is increased. We find a minimal box length of $L \simeq 1.6$ fm, below which chiral perturbation theory cannot be safely applied. Finally, we discuss the infinite volume properties of our quark propagator. We determine the chiral condensate in Sec. V A, comment on possible analytic structures in Sec. V B and give results for the corresponding pion mass and decay constant in Sec. V C. We summarize and conclude in Sec. VI.

II. CHIRAL SYMMETRY BREAKING IN A BOX

Before we embark on our investigation, let us recall the finite volume behavior of the chiral condensate, as this is the order parameter of dynamical chiral symmetry breaking, [15]. The fermion propagator in its spectral representation is given by

$$S_A(x, y) = \sum_n \frac{u_n(x)u_n^\dagger(y)}{m - i\lambda}, \tag{1}$$

where $u_n(x)$ and λ_n are eigenfunctions and eigenvalues of the Euclidean Dirac operator, $Du_n(x) = \lambda_n u_n(x)$. The gauge field A is treated as an external field. These eigenfunctions occur either as zero modes or in pairs of opposite eigenvalues. Setting $x = y$, integrating over x and neglecting the zero mode contributions, one obtains

$$\frac{1}{V}\int_V S_A(x, x) = -\frac{2m}{V}\sum_{\lambda_n > 0}\frac{1}{m^2 + \lambda_n^2}. \tag{2}$$

The quark condensate can be deduced by averaging the

left-hand side of this equation over all gauge field configurations and then taking the infinite volume limit to give

$$\langle \bar{q}q \rangle = -2m \int_0^\infty d\lambda \frac{\rho(\lambda)}{m^2 + \lambda^2}, \tag{3}$$

where $\rho(\lambda)$ is the mean level density of the spectrum, which becomes dense in the infinite volume limit. In the chiral limit, $m \to 0$, only the infrared part of the spectrum contributes and one finally arrives at the Banks-Casher relation [16]

$$\langle \bar{q}q \rangle = -\pi\rho(0). \tag{4}$$

If the two limits are interchanged, i.e. if one takes the chiral limit before the infinite volume limit, one has a discrete sum in Eq. (2) and the infrared part of the spectrum cannot trigger a nonvanishing chiral condensate: chiral symmetry is restored. If, however, at a given volume the explicit quark mass m is not too small, one can still observe the spontaneous formation of a quark condensate. If the factor $(m^2 + \lambda_n^2)^{-1}$ varies only slightly with n, the sum in Eq. (2) can still be replaced by an integral and Eq. (4) remains valid. For this to be a legitimate approximation one needs $m \gg \Delta\lambda \sim 1/V\rho(\lambda) = \pi/(V|\langle\bar{q}q\rangle|)$, at the lower end of the spectrum. Thus one obtains the condition

$$Vm|\langle\bar{q}q\rangle| \gg \pi. \tag{5}$$

To get a feeling for this condition, note that for a typical value of the chiral condensate of $|\langle\bar{q}q\rangle| = (0.25 \text{ GeV})^3$ and a volume of $V = (5 \text{ fm})^4$ the quark mass has to be of the order $m \gg 5 \cdot 10^{-4}$ GeV, which is well satisfied for all quark masses of physical interest. Whether there are sizeable modifications to the corresponding quark propagator due to the box is however a different question, as we shall see in Sec. IV B.

Chiral perturbation theory builds upon the chiral limit, i.e. it can only be applied on volumes large enough such that small quark masses remain accessible. Correspondingly the chiral expansion parameter $p/(4\pi f_\pi)$ has to be small. On a torus the bosonic degrees of freedom have momenta $\mathbf{p} = 2\pi\mathbf{n}/L$ with $\mathbf{n}$ a vector of integers. Small nonzero momenta are therefore only present if the condition

$$L >> \frac{1}{2f_\pi} \sim 1 \text{ fm} \tag{6}$$

is satisfied. *A priori* there is no way to say by how much L has to exceed 1 fm [7]. In Sec. IV C we will see that this scale can be estimated using the quark-SDE on a torus.

III. THE QUARK SCHWINGER-DYSON EQUATION ON A TORUS

In Euclidean momentum space, the renormalized dressed ghost, gluon and quark propagators in the Landau gauge are given by
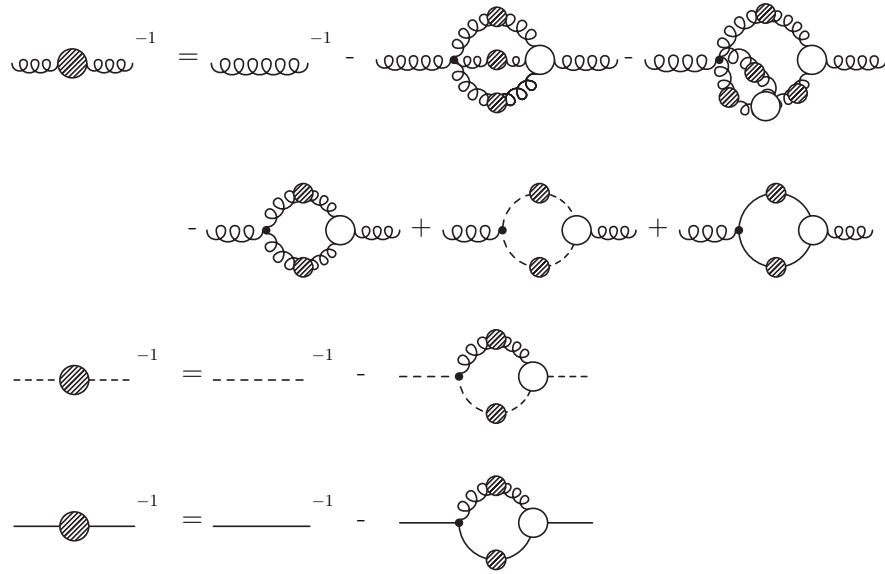
FIG. 1.   The coupled set of Schwinger-Dyson equations for the gluon, ghost and quark propagators.

$$D^G(p^2) = -\frac{G(p^2)}{p^2}, \tag{7}$$

$$D_{\mu\nu}(p) = \left(\delta_{\mu\nu} - \frac{p_\mu p_\nu}{p^2}\right)\frac{Z(p^2)}{p^2}, \tag{8}$$

$$S(p) = \frac{Z_f(p^2)}{i\not{p} + M(p^2)} \tag{9}$$

Here the ghost dressing function $G(p^2)$, the gluon dressing function $Z(p^2)$ and the quark wave function renormalization $Z_f(p^2)$ also depend on the renormalization point μ^2, whereas the quark mass function $M(p^2)$ is a renormalization group invariant. These propagators are given by their corresponding Schwinger-Dyson equations shown diagrammatically in Fig. 1. Since we aim to analyze a quenched lattice quark propagator we will also work in the quenched approximation in the SDE approach and so neglect the quark loop in the gluon-SDE. An estimate of unquenching effects for the propagators and for light meson observables can be found in Ref. [17].

On a compact manifold, the ghost, gluon and quark fields have to obey appropriate boundary conditions in the time direction. These have to be periodic for the gluon and ghost fields,[1] and antiperiodic for the quarks. It is convenient, though not necessary, to choose the same conditions in the spatial directions.[2] We choose the box to be of equal length in all directions, $L_1 = L_2 = L_3 = L_4 \equiv L$, and denote the corresponding volume $V = L^4$. Together

_____

[1]The condition for the ghost field can be read off easily from its BRST-transformation [9].
[2]Different conditions in the spatial directions have been explored in [18,19].

with the boundary conditions this leads to discretized momenta in momentum space. Thus all momentum integrals appearing in the Schwinger-Dyson equations are replaced by sums over Matsubara modes. Since the ghost and gluon SDE on a torus have been investigated in detail in Refs. [9,20], we only discuss the quark-SDE here. On the manifold R^4, the quark-SDE can be written as

$$S^{-1}(p) = Z_2[S^0(p)]^{-1} - C_F\frac{Z_2}{\tilde{Z}_3}\frac{g^2}{(2\pi)^4}$$

$$\times \int d^4k \gamma_\mu S(k)\Gamma_\nu(k,p)D_{\mu\nu}(p-k), \tag{10}$$

where the factor $C_F = 4/3$ stems from the color trace and we have introduced a reduced quark-gluon vertex $\Gamma_\nu(k,p)$, by defining $\Gamma_{\nu,i}^{\text{full}}(k,p) = ig\frac{\lambda_i}{2}\Gamma_\nu(k,p)$. The bare quark propagator is given by $[S^0(p)]^{-1} = i\gamma \cdot p + Z_m m(\mu^2)$, where $m(\mu^2)$ is the renormalized current quark mass. The wave function and quark mass renormalization factors, Z_2 and Z_m, are determined in the renormalization process. The ghost renormalization factor, $\tilde{Z}_3$, will be discussed below, when we introduce our expression for the quark-gluon vertex. The quark mass function $M(p^2)$ and the wave function $Z_f(p^2)$ can be extracted from Eq. (10) by suitable projections in Dirac-space.

Note that the quark propagator determined from Eq. (10) is independent of the regularization procedure. In our numerical calculations we use a subtracted version of Eq. (10) and an O(4)-invariant UV-cutoff (for details see e.g. Ref. [21]). It is a simple matter to explicitly verify numerically (and also analytically) that the resulting quark propagator is independent of the cutoff, which therefore can be sent to infinity at the end of each calculation. The quark-SDE, Eq. (10), therefore represents not only the

infinite volume limit but also the continuum limit (in coordinate space) of any representation of the SDE on a compact manifold. We will use the phrase infinite volume/continuum limit in the following to indicate this simultaneous removal of both an ultraviolet and an infrared cutoff.

On a torus with antiperiodic boundary conditions for the quark fields, the momentum integral changes into a sum of Matsubara modes,

$$\int \frac{d^4q}{(2\pi)^4}(\cdots) \longrightarrow \frac{1}{L^4} \sum_{n_1,n_2,n_3,n_4} (\cdots), \quad (11)$$

counting momenta $\mathbf{q_n} = \sum_{i=1..4}(2\pi/L)(n_i + 1/2)\hat{e}_i$, where $\hat{e}_i$ are Cartesian unit vectors in Euclidean momentum space. For the numerical treatment of the equations it is convenient to rearrange this summation so that it represents a spherical coordinate system [20], see Fig. 2 for an illustration. We then write

$$\frac{1}{L^4} \sum_{n_1,n_2,n_3,n_4} (\cdots) = \frac{1}{L^4} \sum_{j,m} (\cdots), \quad (12)$$

where j counts spheres with $\mathbf{q_n}\mathbf{q_n} = $ const, and m numbers the grid points on a given sphere. The corresponding momentum vectors are denoted $\mathbf{q}_{m,j}$ and their absolute values are given by $q_{m,j} = |\mathbf{q}_{m,j}|$. It is then a simple matter to introduce an $O(4)$-invariant cutoff by restricting j to an interval [1,N]. The resulting quark-SDE is given by
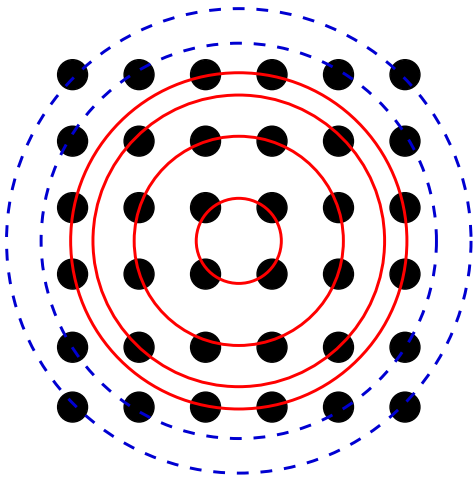

FIG. 2 (color online).   Two-dimensional sketch of the momentum grid dual to the four-torus for a fixed Cartesian momentum cutoff. The hyperspheres depicted by dashed lines are not complete in the sense that additional momentum points on these spheres are generated if the cutoff is increased. The O(4)-invariant cutoff used in our calculations sums only over complete hyperspheres, which are indicated by fully drawn circles.

$$S^{-1}(p_{i,l}) = Z_2[S^0(p_{i,l})]^{-1} - C_F \frac{Z_2}{\tilde{Z}_3} \frac{g^2}{L^4}$$

$$\times \sum_{j,m}^{N} \gamma_\mu S(k_{j,m}) \Gamma_\nu(k_{j,m}, p_{i,l}) D_{\mu\nu}(p_{i,l} - k_{j,m}). \quad (13)$$

Note that the momentum argument of the gluon propagator is a difference of two antiperiodic Matsubara momenta and thus lives on a momentum grid corresponding to periodic boundary conditions as it should.

The quark Schwinger-Dyson equations, Eqs. (10) and (13), can be solved numerically employing well-established methods once the input from the Yang-Mills sector, the gluon propagator $D_{\mu\nu}$ and the fully dressed quark-gluon vertex $\Gamma_\nu(k, p)$ are specified. Our numerical method on the torus is outlined in Ref. [9], the corresponding continuum method as well as details on the renormalization procedure of the quark-SDE are given in Ref. [21]. The truncation scheme of the Yang-Mills sector is discussed in Refs. [20].

IV. NUMERICAL RESULTS FOR THE PROPAGATORS

A. Yang-Mills sector and parameter fitting

Before we discuss our ansatz for the quark-gluon vertex, let us shortly summarize the results of Ref. [9] for the ghost and gluon propagators on the torus. In Fig. 3, the numerical solutions for the gluon propagator $Z(p^2)/p^2$ (left diagram) and the ghost dressing function $G(p^2)$ (right diagram) in the continuum and on a torus[3] are displayed together with the results of recent lattice simulations. Overall there is very good agreement between the DSE-solutions on the compact manifold and the lattice data. However, the infrared (IR) behavior of the DSE-solutions on R^4 is qualitatively different, although the truncation scheme used in solving the SDEs is the same. The ghost dressing function in Fig. 3 diverges in the infinite volume/continuum limit, whereas it stays finite on the compact manifold. For the gluon propagator, this difference can be expressed in terms of an infrared power law,

$$Z(p^2) \sim (p^2)^{2\kappa}. \quad (14)$$

One obtains $\kappa \approx 0.5$ (IR-finite) on a compact manifold (even for very large volumes), whereas $\kappa \approx 0.596$ (IR-vanishing) on R^4 in agreement with analytical results [20,22–24]. This is a decisive difference, since it can be shown that an infrared vanishing gluon propagator cannot have a positive definite spectral function and is therefore

---

[3]There are two slight changes compared to the treatment in Ref. [9]: we adapted the overall scale to match the lattice results and the ultraviolet cutoff has been increased from $\Lambda = 2.47$ GeV to $\Lambda = 3.60$ GeV in order to minimize artifacts due to the cutoff.
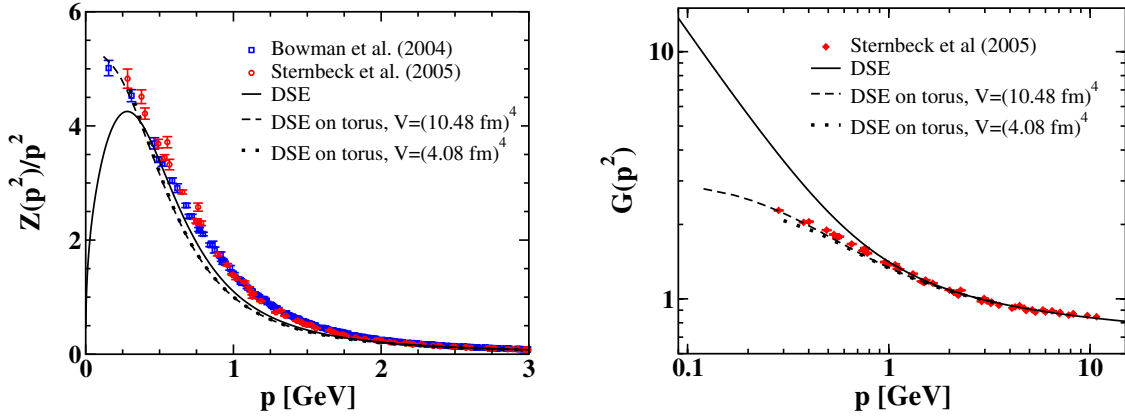
FIG. 3 (color online).   The results for gluon and ghost from Dyson-Schwinger equations in the continuum and on the torus are compared with the lattice data of Refs. [10,11]

confined. Indeed, Zwanziger has argued that the lattice gluon propagator should vanish in the continuum limit [25] and therefore be confined as an effect of the proximity of the Gribov-horizon for low momentum gauge field configurations. However, no statement could be made as to the rate with which the continuum limit behavior is approached. Current extrapolations of lattice data to the infinite volume limit (on large asymmetric lattices) are somewhat ambivalent. Whereas an extrapolation of the gluon dressing function leads to $\kappa \approx 0.52$ (IR-vanishing), one obtains $\kappa = 0.5$ (IR-finite) from an extrapolation of the corresponding gluon propagator [26]. Therefore, it seems as if there is a genuine difference between propagators on different manifolds, which has to be taken into account when extrapolating to infinite volumes. The differences shown in Fig. 3 may serve as a measure of the upper limit of these effects.

The (quenched) solution for the gluon propagator on both type of manifolds is used directly as input in the corresponding quark-SDE on a torus and in the infinite volume/continuum limit. What remains then is to specify an explicit expression for the quark-gluon vertex. Here we follow the strategy of Ref. [14] and employ a parametrization of the vertex such that the (quenched) lattice results for the quark propagator are reproduced by the gap equation. Our ansatz for the vertex is

$$\Gamma_\nu(k, \mu^2) = \gamma_\nu \Gamma_1(k^2)\Gamma_2(k^2, \mu^2)\Gamma_3(k^2, \mu^2) \qquad (15)$$

where k^2 is the gluon momentum and μ^2 is the renormalization scale. The ansatz depends on the gluon momentum only and is thus the simplest possible form that respects charge conjugation symmetry. Furthermore, this choice of momentum dependence ensures the existence of a corresponding kernel in the Bethe-Salpeter equation for mesons in accordance with the axial-vector Ward-Takahashi identity, cf. Sec. V C. The three components of this ansatz are given by

$$\Gamma_1(k^2) = \frac{\pi \gamma_m}{\ln(k^2/\Lambda_{\text{QCD}}^2 + \tau)}, \qquad (16)$$

$$\Gamma_2(k^2, \mu^2) = G(k^2, \mu^2)G(\zeta^2, \mu^2)$$
$$\times \tilde{Z}_3(\mu^2)h[\ln(k^2/\Lambda_g^2 + \tau)]^{1+\delta} \quad (17)$$

$$\Gamma_3(k^2, \mu^2) = Z_2(\mu^2)\frac{a(M) + k^2/\Lambda_{\text{QCD}}^2}{1 + k^2/\Lambda_{\text{QCD}}^2}, \qquad (18)$$

where $\delta = -9/44$ is the (quenched) one-loop anomalous dimension of the ghost, $\gamma_m = 12/33$ the corresponding anomalous dimension of the quark and $\tau = e - 1$ acts as a convenient infrared cutoff for the logarithms. It is well known that the effective interaction $g^2Z\Gamma_1\Gamma_2\Gamma_3$ in the quark-SDE has to approach the running coupling in the ultraviolet momentum regime [27]. In our ansatz this UV-part of the interaction is represented by Γ_1. The scale Λ_{QCD} is scheme dependent. Here, since we fit to the lattice data of Refs. [12,13], its value corresponds to the momentum subtraction scheme used therein. The product $Z\Gamma_2\Gamma_3$ goes to a constant for large momenta, since the ultraviolet behavior of the ghost and gluon dressing functions is given by

$$G(z) = G(s)\left[\omega \log\left(\frac{z}{s}\right) + 1 \right]^\delta,$$
$$Z(z) = Z(s)\left[\omega \log\left(\frac{z}{s}\right) + 1 \right]^\gamma, \qquad (19)$$

with $\omega = \beta_0\alpha(s)/(4\pi) = 11N_c\alpha(s)/(12\pi)$ and a large scale s. The anomalous dimensions of the ghost and the gluon dressing functions in $Z\Gamma_2\Gamma_3$ combine to $\gamma + \delta = -1 - \delta$, which is balanced by the explicit logarithm in Γ_2. The scale Λ_g in Eq. (17) represents a possibly scheme-dependent scale inherent in the Yang-Mills part of the interaction, which is related to the analytic structure of the gluon propagator. The coefficient h is fixed such that the ultraviolet behavior of the resulting running coupling

matches the one calculated on the lattice in Ref. [11]. The renormalization group invariant $G(\zeta^2, \mu^2)\tilde{Z}_3(\mu^2)$ with the arbitrary scale ζ is introduced to impose the correct cutoff- and renormalization point dependences of the effective interaction in the quark-SDE. Together, the product $\Gamma_1\Gamma_2$ represents the non-Abelian content of the quark-gluon vertex as expressed in its Slavnov-Taylor identity (STI) given by [28]

$$G^{-1}(k^2)k_\nu\Gamma_\nu(q, k) = S^{-1}(p)H(q, p) - H(q, p)S^{-1}(q), \quad (20)$$

where q and p are the quark momenta. This identity enforces the presence of the ghost factor $G(k^2)$ in Γ_2, which makes the quark-gluon vertex an infrared singular object, similar to the three- and four-gluon vertices [29]. The remaining part of $\Gamma_1\Gamma_2$ is infrared finite and can be interpreted as a model for the ghost-quark scattering kernel $H(q, p)$. The dependency of the vertex on the quark wave function Z_f through the inverse quark propagators in the STI is taken care of by Γ_3, the form of which is chosen appropriately. The extra factor Z_2 is vital in ensuring multiplicative renormalizability of the quark-SDE.[4] The dependence of this part of the vertex on the quark mass is expressed in terms of the function

$$a(M) = \frac{a_1}{1 + a_2 M(\zeta^2)/\Lambda_{\mathrm{QCD}} + a_3 M^2(\zeta^2)/\Lambda_{\mathrm{QCD}}^2}. \quad (21)$$

In order to preserve multiplicative renormalisability of the quark-SDE, it is important that the scale ζ at which the quark mass function is read off (and also the ghost factor in Γ_1) is not correlated with the renormalization point. Instead it should be a fixed scale sufficiently far into the ultraviolet region that volume effects are negligible. In our calculations we use $\zeta = 2.9$ GeV.

To fit the various parameters in our model interaction we solve the quark-SDE on a torus employing a momentum range similar to that used in the lattice calculations of Refs. [12,13]. In the SDE this corresponds to a 24^4 (36^4) lattice in momentum space with a smallest momentum of 304 MeV (200 MeV) corresponding to a box-size of $L_1 = L_2 = L_3 = L_4 = L = 2.04$ fm $(L = 3.10$ fm) for the staggered (overlap) quarks. We first determine the parameters h, Λ_g and Λ_{QCD} by fitting the "Yang-Mills part" $\Gamma_1\Gamma_2$ of our vertex model to the ultraviolet part of the lattice running coupling from Ref. [11], which agrees with the two-loop results from perturbation theory. This fit is not unique but gives a range of pairs $(\Lambda_g, \Lambda_{\mathrm{QCD}})$ related to the value of h. We then choose current quark masses $m(\mu^2)$ such that the ultraviolet behavior of the lattice quark mass functions are reproduced by the solutions of the quark-SDE. As the ultraviolet behavior of the quark mass func-

[4]Note that the effective interaction of Ref. [14] fails to ensure multiplicative renormalizability and is therefore only valid at the fixed renormalization point chosen in their work.

tion is determined by the ultraviolet behavior of the input interaction, we find the same result for each pair $(\Lambda_g, \Lambda_{\mathrm{QCD}})$. This merely reflects the fact that the ultraviolet behavior of the quark mass function is controlled by resummed perturbation theory and is therefore model independent. We then deduce values of the function $a(m)$ in Eq. (21) such that the lattice quark mass functions are reproduced. Although this is possible for all values of the pairs $(\Lambda_g, \Lambda_{\mathrm{QCD}})$, the corresponding quark wave functions $Z_f(p^2)$ favor a small range of values for Λ_{QCD} and Λ_g. Finally we fix the coefficients $a_{1,2,3}$ and determine the values of the quark mass function $M(\zeta)$ corresponding to different renormalized current quark masses $m(\mu^2)$. Our final best parameter sets together with the quark masses are tabulated in Tables I and II. Note that the bare staggered quark masses are smaller than the renormalized quark masses from the SDE, whereas the corresponding bare overlap quark masses are larger. Comparing the functions $M_{\mathrm{SDE}}(m_{\mathrm{lattice}})$ for both formulations we find agreement if the bare staggered quark masses are multiplied by a factor 1.70. No additional additive corrections, which recently have been identified as a consequence of taste symmetry breaking [30], are necessary.

A few comments on the quality of our fits are in order. The scales Λ_{QCD} and Λ_g cannot be determined very well; we estimate the error in these scales to be of the order of 30%. With the given values for these scales, the uncertainty in the parameter h is then only related to the (small) error bars of the lattice coupling from Ref. [11], i.e. of the order of 2%. The errors for our values of the parameters a_1, a_2, a_3 are correlated to both the error in the determination of the current quark mass from the lattice data and the error bars of the lattice data in the infrared momentum regime. This leads to uncertainties of the order of a few percent. We have also performed fits to $a(M)$ setting $a_3 = 0$, thereby testing the possible redundancy of this parame-

TABLE I. Renormalized quark masses in the SDE on the torus at $\zeta = 2.9$ GeV compared with the bare quark masses on the lattice from Refs. [12,13]. Note that the bare staggered quark masses are smaller than the renormalized quark masses from the SDE, whereas the corresponding bare overlap quark masses are larger (cf. the discussion in the text).

	staggered			overlap			
m_{lattice} (GeV)	0.028	0.057	0.114	0.090	0.140	0.210	0.300
$M_{\mathrm{SDE}}(\zeta^2)$(GeV)	0.044	0.080	0.151	0.076	0.112	0.162	0.225

TABLE II. Parameters used in the vertex model, Eqs. (15)–(18).

	h	Λ_g(GeV)	Λ_{QCD}(GeV)	a_1	a_2	a_3
staggered	1.33	1.50	0.35	25.30	4.80	-1.39
overlap	1.31	1.50	0.35	25.58	3.44	2.23

ter. The fits become worse in the range where lattice data are available, but still might be of tolerable quality. However, there is a nontrivial effect which convinced us of the importance of the parameter a_3: if $a_3 = 0$ we obtained vastly different values for $a(M)$ in the chiral limit for the staggered and the overlap data. However, fitting a_3 as a free parameter these values almost coincide. As a consequence, one obtains almost identical quark propagators if the infinite volume/continuum limit and then the chiral limit are performed. On general grounds the overlap and staggered formulation of quarks on the lattice should coincide in the continuum limit. Possible residual scheme dependences at finite current quark masses necessarily vanish in the chiral limit, provided there are no additive mass corrections (see above). This is exactly what we see if a_3 is included as a free parameter. All qualitative conclusions of our paper do not depend on the details of the fits and are stable with respect to a variation of the parameters within the errors given above. For our quantitative results we have included these uncertainties in our estimate of the overall error margins. Unfortunately, it is extremely difficult to give a quantitative estimate of the systematic truncation error, i.e. an estimate of possible changes once subleading structures of the vertex are taken into account. Wherever possible we have tried to assess such effects on a qualitative basis.

B. The quark propagator at finite and infinite volume

In Fig. 4 we compare our results from the SDE with the lattice data. The solutions for the quark mass function $M(p^2)$ from the SDE can be nicely fitted to the lattice results in both, the staggered and the overlap formulation. For the quark wave function $Z_f(p^2)$ in the staggered formulation, shown in the upper right diagram of Fig. 4, we observe a slightly larger spread in the SDE solutions than on the lattice.[5] The same is true when compared to the overlap data, although here in addition we observe a larger fall in the infrared. We have tried to reproduce this steeper decrease by considering various modifications of our model interaction, Eqs. (15)–(18), but have not succeeded. In particular introducing additional ghost factors, which correspond to an even more singular vertex in the continuum, does not improve the situation. It seems to us, that such a fall can only be reproduced when further tensor structures of the quark-gluon vertex is taken into account. Indeed, employing the Ball-Chiu construction [31]

$$\Gamma_\nu^{BC} = \frac{1}{2}(A(p^2) + A(q^2))\gamma_\nu + \frac{1}{2}(A(p^2) - A(q^2))$$
$$\times \frac{(\slashed{p} + \slashed{q})(p+q)_\nu}{p^2 - q^2} + i(B(p^2) - B(q^2))\frac{(p+q)_\nu}{p^2 - q^2}$$
$$(22)$$

_____

[5]The parametrization used in Ref. [14] leads to a similar large spread (not explicitly shown in their paper).

instead of γ_ν (and modified parameters $a_{1,2,3}$), we could at least reproduce the sharper decrease at small masses. However, as can be seen in Fig. 4, the problem remains for large masses. It is therefore not clear to us, whether the sharper low momentum decrease in the overlap data should be taken seriously and really interpreted as an indication of the importance of a richer tensor structure in the quark-gluon vertex, or whether one should prefer the staggered data and conclude that the γ_ν-part of the vertex is sufficient to reproduce the lattice results. We leave this question open for future investigations in both the SDE-formalism and on the lattice, and proceed using our simple construction, Eqs. (15)–(18).

To assess finite volume effects we now compare the lattice/SDE-results on the compact manifold with the infinite volume/continuum limit. To this end we solve the quark-SDE in the continuum employing our lattice inspired ansatz for the quark-gluon vertex and the continuum solutions for the ghost and gluon propagators, discussed in Sec. IVA, as input. This procedure does take into account finite volume effects from three different sources: first, from the gluon propagator; second, from the quark-gluon vertex via its ghost content in Γ_2; and third, effects generated by the quark-SDE itself. The parameters of the fitted quark-gluon interaction are kept fixed, as are the renormalized current quark masses. In Fig. 5 we compare our results in the infinite volume limit to the lattice data. We observe finite volume effects for momenta smaller than 1 GeV. The most pronounced effects occur in the infrared momentum region, where the continuum mass functions approach finite values at vanishing momentum which are substantially larger than anticipated from the lattice data alone. We conclude that lattice data underestimate the quark mass that is dynamically generated by a substantial amount. The absolute size of this effect is approximately the same for all quark masses we have investigated, so the relative size becomes smaller for heavier quarks. Exactly as expected heavier quarks fit on finite volumes most readily, but here we have deduced the size of the volume effects for all masses.

Another interesting effect occurs for small momenta: the quark mass function in the chiral limit is actually larger than the one for the smallest nonzero current quark mass. This effect has also been observed directly from the quenched staggered lattice data [32]. The effect is more pronounced for the staggered quarks, as can be seen by comparing the two diagrams of Fig. 6 at small quark masses. There we show the quark mass function at a given momentum, $M_{IR} := M(p^2 = 0.0924 \text{ GeV}^2)$, plotted as a function of the current quark mass. Apart from small quantitative differences, the qualitative behavior of $M_{IR}(m)$ is similar for both fermion formulations. On the compact manifold, one observes a (small) volume dependence for $2 < L < 3$ fm, which becomes negligible for $L > 3$ fm. However, even then one is still far away from
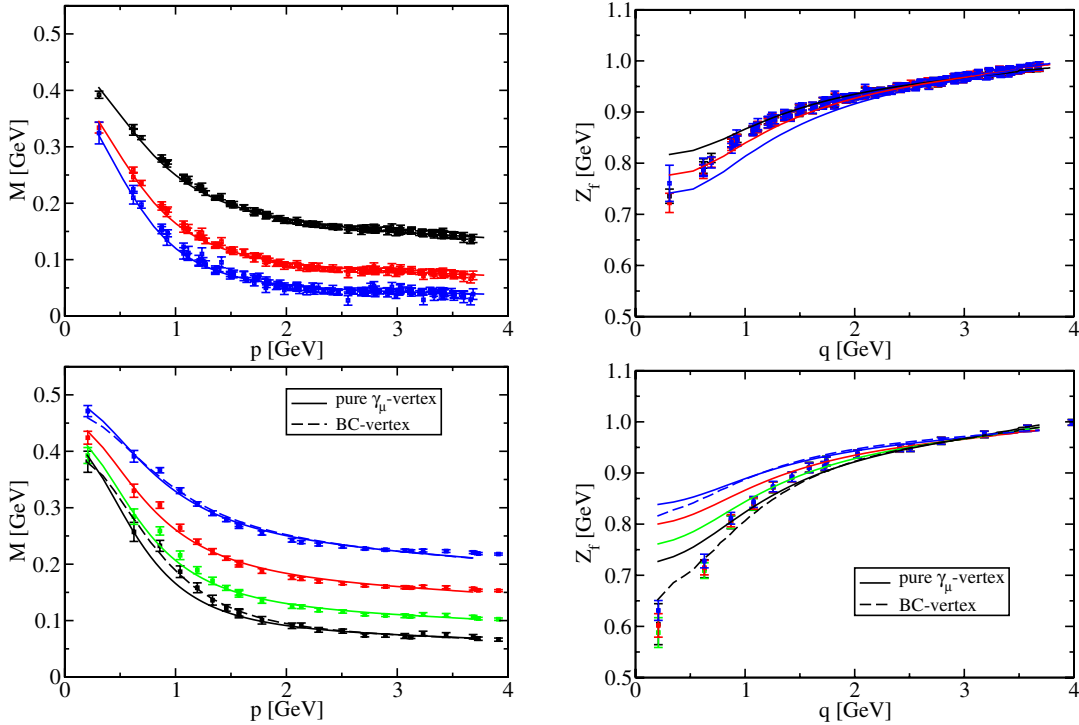
FIG. 4 (color online).   The results for quark mass function M and the wave function Z_f from Dyson-Schwinger equations on the torus compared with lattice data for staggered quarks [12] (upper panel) and overlap quarks [13] (lower panel). The lattice momentum p has been used for the lattice mass functions, whereas the choice of the "kinematical momentum" q corrects for hypercubical artifacts in the lattice wave functions [12,13]. The results for the Ball-Chiu ansatz, Eq. (22), are shown only for the largest and smallest masses of the overlap quark propagator.
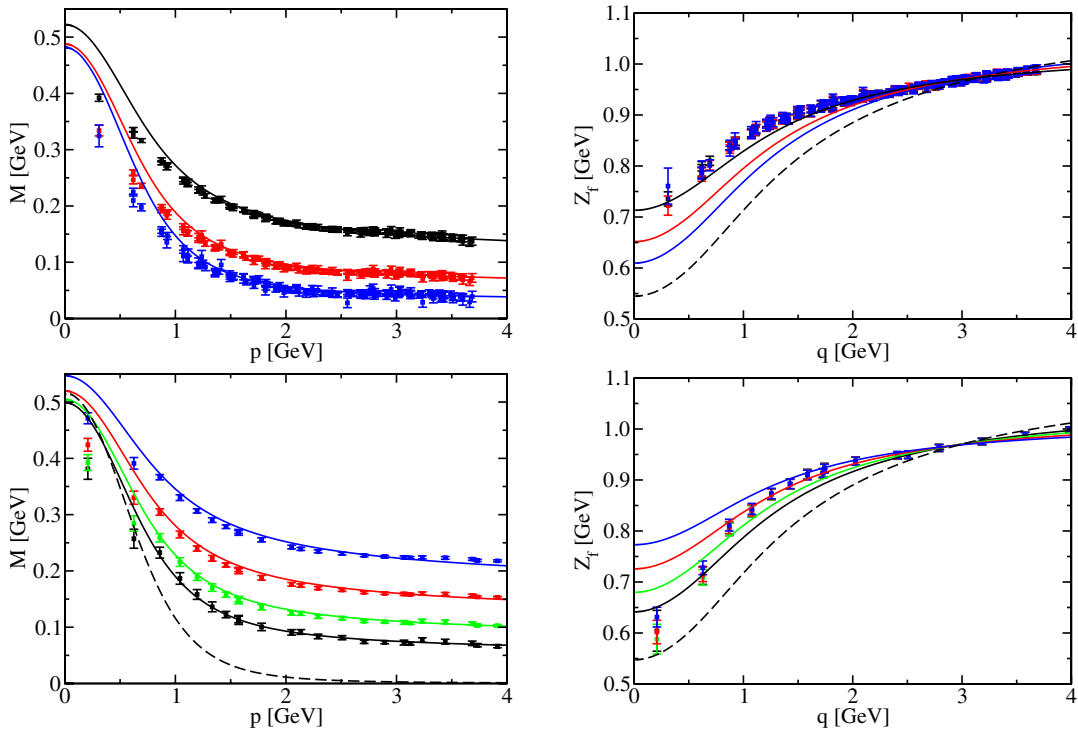

FIG. 5 (color online).   The results for quark mass function M and the wave function Z_f from Dyson-Schwinger equations in the continuum compared with the same lattice data as in Fig. 4 (staggered quarks in the upper panel, overlap quarks in the lower panel). Also shown is the chiral limit (dashed curves).
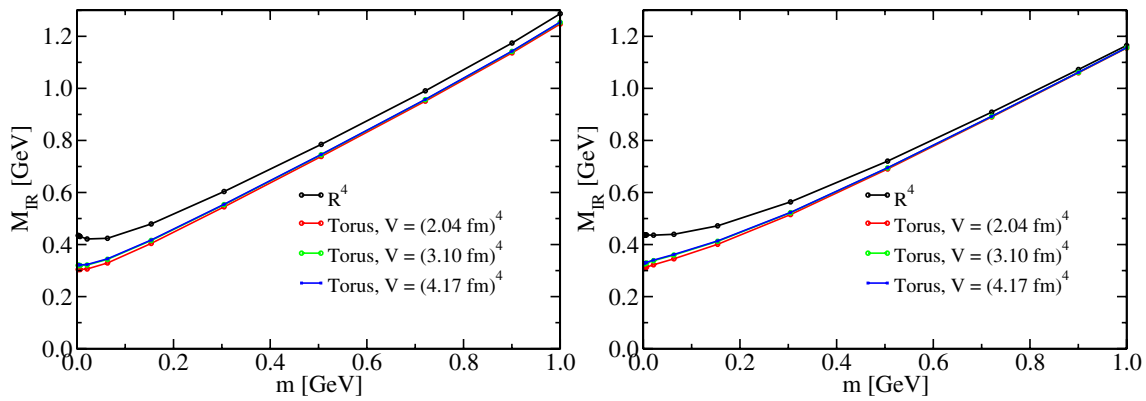
FIG. 6 (color online). The quark mass function at a given momentum $M_{IR}: = M(p^2 = 0.0924 \text{ GeV}^2)$ plotted as a function of the current quark mass $m(\mu^2)$ in the continuum and on tori with different volumes (staggered quarks in the left diagram, overlap quarks in the right diagram).

the infinite volume results. This remaining difference stems from the Yang-Mills sector of the theory: the difference there between the torus and infinite volume results (cf. Fig. 3) has a direct impact on the effective interaction in the quark-SDE and therefore on the results for the quark propagator. The size of this effect depends on the continuum value of the exponent κ [cf. Eq. (14)], which is closely related to the quality of the approximation of the ghost-gluon-vertex in the ghost and gluon SDEs. There are indications that the "true" exponent κ may be closer to $\kappa \approx 0.5$ and therefore closer to the current lattice data than our value $\kappa \approx 0.596$ [23,24,33]. Thus we regard our result as an upper limit for the effects that depend upon the volume.

C. A critical volume for chiral perturbation theory

As discussed above, dynamical chiral symmetry breaking alone cannot occur on a finite volume. A nonvanishing current quark mass satisfying the condition

FIG. 7. The quark mass function for an up/down quark at a given momentum $p = 1$ GeV plotted as a function of the box length.

$$Vm|\langle \bar{q}q \rangle| \gg \pi \qquad (23)$$

has to be present as a "seed" to trigger dynamical mass generation and the formation of a chiral condensate. Chiral perturbation theory, on the other hand, is built upon the chiral limit and therefore can only be applied on volumes large enough such that very small quark masses are feasible. The corresponding condition, discussed above, is

$$L \gg \frac{1}{2f_\pi} \sim 1 \text{ fm.} \qquad (24)$$

We will now give an estimate of how large L has to be in practice. To this end we employ a current quark mass of the order of a typical up/down-quark mass, $M(p^2 = 2.9 \text{ GeV}^2) = 10$ MeV , and determine the mass function $M(p^2)$ at $p^2 = 1$ GeV from solutions on tori with different volumes by linearly interpolating on the corresponding momentum grids. The result is plotted in Fig. 7. We clearly see that the quark mass function grows rapidly in the range $1.0 < L < 1.6$ fm signaling the onset of dynamical chiral symmetry breaking. Above $L = 1.6$ fm, a plateau is reached. This picture does not change when we extract the mass function $M(p^2)$ at smaller momenta p^2 or when we employ even smaller quark masses. Thus a safe value for L should be at least

$$L_{\chi PT} \simeq 1.6 \text{ fm.} \qquad (25)$$

This is a surprisingly small value in light of the condition Eq. (23) and so provides some justification for extending chiral perturbation theory to rather small volumes.

V. PROPERTIES OF QUARKS AND PIONS IN THE INFINITE VOLUME/CONTINUUM LIMIT

A. The chiral condensate

Having studied the volume dependence of the quark propagator in some detail, we now focus on R^4 and investigate the quark/meson sector employing our effective
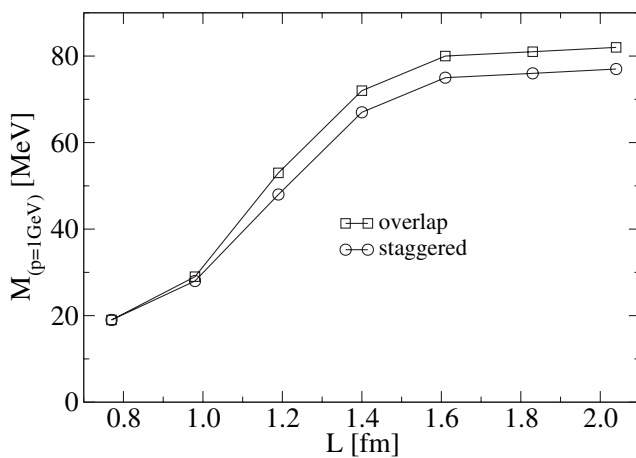
interaction which has been fixed by the lattice input. From the quark propagator S_χ in the chiral limit, we can determine the value of the (renormalization point dependent) chiral condensate using

$$-\langle \bar{q}q \rangle(\mu^2) := Z_2(\mu^2) Z_m(\mu^2) N_c \text{tr}_D \int \frac{d^4 q}{(2\pi)^4} S_\chi(q, \mu^2), \tag{26}$$

where the trace is over Dirac indices. Its value is conveniently determined at a large renormalization scale, converted to the renormalization point independent chiral condensate and then run down to $\mu = 2$ GeV employing the quenched scale $\Lambda_{\text{QCD}}^{\overline{MS}} = 0.225(21)$ MeV [34]. We then obtain the values

$$-\langle \bar{q}q \rangle_{\text{overlap}}^{\overline{MS}}(\mu^2) = (252.6 \pm 5.0 \text{ MeV})^3,$$
$$-\langle \bar{q}q \rangle_{\text{staggered}}^{\overline{MS}}(\mu^2) = (253.0 \pm 5.0 \text{ MeV})^3, \tag{27}$$

which are in very good agreement with each other. The error given is an estimate of combined numerical and scale uncertainties. It is a quite interesting and satisfying result that the continuum chiral limit quark propagators of the staggered and overlap fermions agree very well with each other. It is furthermore interesting to compare our value for the chiral condensate with recent results using other methods on the lattice. Gimenez *et al.* [35] find the value $(265 \pm 27 \text{ MeV})^3$ from an operator product expansion employing an $O(a)$-improved quenched Wilson action. Wennekers and Wittig [36] quote $(285 \pm 9 \text{ MeV})^3$, determined from a quenched overlap action. Both values are in fair agreement with each other and with our result. McNeile [37] recently obtained the value $(259 \pm 27 \text{ MeV})^3$ from a chiral Lagrangian with parameters fixed by lattice data employing $N_f = 2 + 1$ staggered sea quarks, thus indicating that unquenching effects in the chiral condensate may be small. This is in excellent agreement with the prediction in the SDE/BSE-approach [17,21].

B. On the analytical properties of the quark propagator

The analytic properties of the quark propagator can in part be read off from the corresponding Schwinger function

$$\sigma(t) = \int d^3 x \int \frac{d^4 p}{(2\pi)^4} \exp(ip \cdot x) \sigma_{S,V}(p^2), \tag{28}$$

where $\sigma_{S,V}$ are the scalar and the vector parts, respectively, of the dressed quark propagator. (This method has a long history, see e.g. [38–44] and references therein). According to the Osterwalder-Schrader axioms of Euclidean field theory [45], this function has to be positive to allow for asymptotic states in the physical sector of the state space of QCD. Conversely, positivity violations in the Schwinger function show that the corresponding asymptotic states (if present) belong to the unphysical part of the
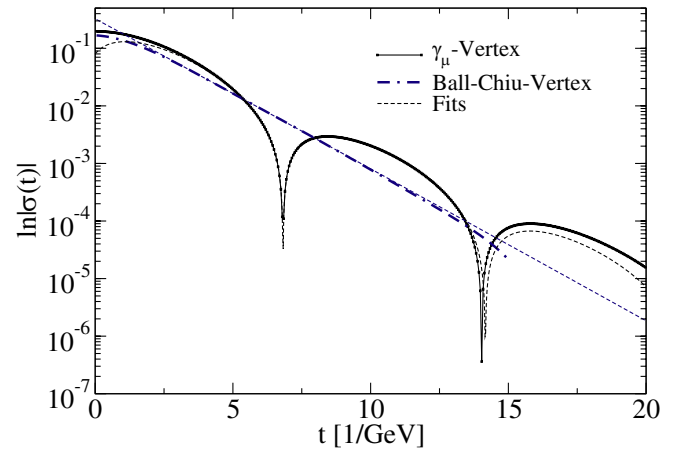

FIG. 8 (color online). The logarithm of the Schwinger function $\ln(|\sigma(t)|)$ of the chiral limit quark propagator as a function of time. Shown are results for the staggered and overlap quark, (i) employing the ansatz Eq. (15) for the quark-gluon vertex and (ii) substituting the Ball-Chiu construction, Eq. (22), for γ_ν. The respective curves for the staggered and overlap quarks are indistinguishable in the plot. We compare the results to fits of the function Eq. (29).

state space. Thus positivity violations constitute a sufficient condition for confinement. Our results for the Schwinger function of the chiral limit quark propagator in the staggered and overlap formalisms are shown in Fig. 8. The Schwinger functions of the two formulations agree extremely well and are indistinguishable in the plot. Let us first discuss the result obtained with our simple vertex construction involving only the vector part γ_μ of the vertex. The cusp at $t = 6.76$ GeV$^{-1} = 1.33$ fm indicates a node in the Schwinger function corresponding to positivity violations at a scale in rough agreement with the size of hadrons. An excellent fit to the Schwinger function is obtained using the form [46]

$$\sigma(t) = b_0 \exp(-b_1 t) \cos(b_2 t + b_3), \tag{29}$$

which corresponds to a pair of complex conjugate poles of the propagator in the timelike momentum plane. These poles correspond to a "quark mass" given by $m = b_1 \pm ib_2$, which in our case is $m = 516(20) \pm i428(20)$ MeV. Taken at face value this means that the lattice quark propagator is confined (this is also the conclusion drawn by Bhagwat *et al.* [14]). However, there is a caveat: it has been shown in Ref. [44] that the presence of a sufficiently strong scalar part in the quark-gluon vertex can have a strong influence on the analytic structure of the solution of the quark-SDE. Indeed if we employ the Ball-Chiu construction, Eq. (22), instead of γ_μ we obtain an exponentially decaying Schwinger function denoted by the dash-dotted line in Fig. 8. Such a function corresponds to a positive definite quark propagator with a pole on the real axis at $m = 632(20) \pm i0(2)$ MeV (within numerical accuracy). This shows that the analytic structure of the quark

propagator depends strongly on the details of the structure of the quark-gluon vertex and one cannot make definite statements from fitted interactions alone. First attempts on the lattice [47] as well as in the SDE/BSE approach [48–50] have been made to study the tensor structure of the quark-gluon vertex in more detail. Still, more effort is needed before definitive conclusions about the analytic structure of the quark propagator are in sight.

C. Pion mass and decay constant from the lattice interaction

Finally, we have determined the mass and the decay constant of the pion employing the effective quark-gluon interaction fitted to the lattice data. The pion is described by the homogeneous Bethe-Salpeter equation (BSE)

$$\Gamma^\pi_{\alpha\beta}(p;P) = \int \frac{d^4k}{(2\pi)^4} K_{\alpha\beta;\delta\gamma}(p,k;P)$$
$$\times [S(k_+)\Gamma^\pi(k;P)S(k_-)]_{\gamma\delta} \qquad (30)$$

where

$$\Gamma^\pi(p;P) = \gamma_5[E^\pi(p;P) - \iota\not\!P F^\pi(p;P) - \iota\not\!p G^\pi(p;P)$$
$$- [\not\!P, \not\!p]H^\pi(p;P)], \qquad (31)$$

is the Bethe-Salpeter amplitude of the pion, K is the Bethe-Salpeter kernel and the momenta $k_+ = k + \xi P$ and $k_- = k + (\xi - 1)P$ are such that the total momentum $P = k_+ - k_-$. All physical results are independent of the momentum partitioning parameter $\xi = [0,1]$. The crucial link between the meson bound states and their quark and gluon constituents is provided by the axial vector Ward-Takahashi identity. It relates the quark self energy to the quark-quark interaction kernel in the BSE and thereby guarantees the Goldstone nature of the pions and kaons [51,52]. In our case the kernel is given by

$$K_{\alpha\beta;\delta\gamma}(p,k;P) \rightarrow [\gamma_\mu]_{\alpha\gamma}$$
$$\times [\gamma_\nu]_{\delta\beta} t_{\mu\nu}(k) Z_2 \frac{Z(k)\Gamma_1(k)\Gamma_2(k)\Gamma_3(k)}{k^2}, \qquad (32)$$

where $t_{\mu\nu}$ is a transverse projector in momentum space and the flavor content of the kernel has been suppressed. To determine the pion mass and wave functions we explicitly solve the quark-SDE in the complex momentum plane, thereby providing the necessary input for the BSE. The BSE is then solved as an eigenvalue equation for eigenvalue one, which provides the wave functions and the pole mass of the pion (all technical details of such a calculation are discussed in detail in Ref. [17]). From the (normalized) wave function the pion decay constant is fixed by

$$f_\pi = \frac{3}{M^2}\text{Tr}_d \int \frac{d^4k}{(2\pi)^4} \Gamma^\pi(k,-P)S(k+P/2)\gamma_5\not\!P(k-P/2). \qquad (33)$$

TABLE III. Results for the renormalized current up/down quark mass, the mass of the pion and the pion decay constant employing the quark-gluon interaction fitted to the lattice data. The evolution of the quark mass has been performed using $\Lambda^{\overline{MS}}_{\text{QCD}} = 0.225(21)$ MeV [34].

	$m^{\mu=2 \text{ GeV}}_{\overline{MS}}$ (MeV)	M_π(MeV)	f_π(MeV)
staggered	4.1 ± 0.3	138.4	83.5
overlap	4.1 ± 0.3	138.7	84.3
experiment	$\cdots$	138.5	92.4

Our results for the pion mass, the corresponding renormalized current quark mass in the $\overline{MS}$-scheme and the pion decay constant are given in Table III. The current quark mass has been determined from the quark-SDE at a large renormalization point, converted into the $\overline{MS}$-scheme and subsequently evolved to $\mu = 2$ GeV employing the same scale as for the chiral condensate, $\Lambda^{\overline{MS}}_{\text{QCD}} = 0.225(21)$ MeV [34]. The errors given in Table III are an estimate of numerical and scale uncertainties. The resulting current quark mass is in the ballpark of the values quoted by the particle data group [53].

Probably the most interesting observable is the pion decay constant, which directly reflects the deficiency of the quenched lattice calculation compared with the real world. Both lattice formulations underestimate the experimental value by roughly 10%. This margin is much smaller than the 30% estimated in Ref. [14], where finite volume effects were not taken into account.

VI. SUMMARY

In summary, we have investigated the properties of a quenched lattice-QCD quark propagator from staggered quarks [12] and from an overlap quark action [13] in Landau gauge. We employed a coupled set of Schwinger-Dyson equations for the ghost, gluon and quark propagators on compact manifolds and in the infinite volume/continuum limit to study finite volume effects in the propagators and to determine some aspects of dynamical chiral symmetry breaking on a torus. We constructed a model for the quark-gluon vertex such that two sets of staggered and overlap lattice quark propagators are reproduced by the quark gap equation on their respective manifolds.

Comparing results on different volumes with the infinite volume/continuum limit, we found sizeable quantitative but not qualitative differences at small momenta. The continuum mass functions approach finite values at vanishing momentum which are substantially larger than anticipated from the lattice data alone. Thus lattice simulations may underestimate the amount of dynamical quark mass generation in the infrared by as much as 100 MeV. The absolute size of this effect is approximately the same for all quark masses we have investigated, so the relative size becomes smaller for heavier quarks. As a by-product of

this investigation we observed that the bare quark masses in the staggered and overlap formulations are related by a simple multiplicative factor. No additional additive corrections were necessary, which is a signal that taste symmetry violations in the staggered action used in Ref. [12] are negligible [30].

We also assessed the effects of small volumes on dynamical chiral symmetry breaking. Employing a fixed small current quark mass we decreased the volume of the box until we found clear signals of chiral symmetry restoration. These signals occur at the surprisingly small box length of

$$L \simeq 1.6 \text{ fm}, \tag{34}$$

which constitutes a minimal box size below which chiral perturbation theory cannot safely be applied.

With the quark-gluon interaction fixed by the lattice data, we then determined the properties of the quark propagator and pions in the infinite volume/continuum limit. We found a chiral condensate of

$$|\langle \bar{q}q \rangle|_{\overline{MS}}^{2 \text{ GeV}} = (253 \pm 5 \text{ MeV})^3 \tag{35}$$

which compares favorably with values determined with other methods on the lattice. Unfortunately nothing can be said about the analytic structure of the quark propagator. We showed, that the method of fitting a quark-gluon interaction to lattice propagator data is not sufficient to pin down the relative strength of the various tensor components of the vertex, which in turn are necessary to derive reliable statements on the analytic structure of the quark

propagator. Finally, we have determined the pion mass and decay constant employing a rainbow-ladder truncation of the Bethe-Salpeter equation, which incorporates the fitted interaction. We obtained the renormalized up/down quark masses

$$m_{\overline{MS}}^{2 \text{ GeV}} = 4.1 \pm 0.3 \text{ MeV}, \tag{36}$$

which are in the ballpark of the values given in the particle data book [53]. The pion decay constant is roughly 10% smaller than the experimental value. This indicates that quenching effects in the light meson sector are not too large in agreement with previous findings [17].

We have shown how the SDE/BSE approach, once matched to lattice results on finite volumes with appropriate manifolds, can reliably determine infinite volume/continuum predictions for all quark masses, including those of the real world close to the chiral limit: a limit not directly accessible on the lattice.

ACKNOWLEDGMENTS

[1] S. Chandrasekharan and U. J. Wiese, Prog. Part. Nucl. Phys. **53**, 373 (2004).

[2] H. Leutwyler, hep-ph/0008124.

[3] R. Alkofer and L. von Smekal, Phys. Rep. **353**, 281 (2001).

[4] P. Maris and C. D. Roberts, Int. J. Mod. Phys. E **12**, 297 (2003).

[5] W. Detmold, W. Melnitchouk, J. W. Negele, D. B. Renner, and A. W. Thomas, Phys. Rev. Lett. **87**, 172001 (2001).

[6] M. Procura, T. R. Hemmert, and W. Weise, Phys. Rev. D **69**, 034505 (2004).

[7] G. Colangelo, S. Durr, and C. Haefeli, Nucl. Phys. **B721**, 136 (2005).

[8] J. Gasser and H. Leutwyler, Nucl. Phys. **B307**, 763 (1988).

[9] C. S. Fischer, B. Gruter, and R. Alkofer, hep-ph/0506053.

[10] P. O. Bowman *et al.*, Phys. Rev. D **70**, 034509 (2004).

[11] A. Sternbeck, E. M. Ilgenfritz, M. Mueller-Preussker, and A. Schiller, Phys. Rev. D **72**, 014507 (2005).

[12] P. O. Bowman, U. M. Heller, and A. G. Williams, Phys. Rev. D **66**, 014505 (2002).

[13] J. B. Zhang, P. O. Bowman, R. J. Coad, U. M. Heller, D. B. Leinweber, and A. G. Williams, Phys. Rev. D **71**, 014501

(2005); Nucl. Phys. B, Proc. Suppl. **141**, 15 (2005).

[14] M. S. Bhagwat, M. A. Pichowsky, C. D. Roberts, and P. C. Tandy, Phys. Rev. C **68**, 015203 (2003).

[15] H. Leutwyler and A. Smilga, Phys. Rev. D **46**, 5607 (1992).

[16] T. Banks and A. Casher, Nucl. Phys. **B169**, 103 (1980).

[17] C. S. Fischer, P. Watson, and W. Cassing, Phys. Rev. D **72**, 094025 (2005).

[18] S. Aoki, T. Umemura, M. Fukugita, N. Ishizuka, H. Mino, M. Okawa, and A. Ukawa, Phys. Rev. D **50**, 486 (1994).

[19] J. Braun, B. Klein, and H. J. Pirner, Phys. Rev. D **72**, 034017 (2005).

[20] C. S. Fischer, R. Alkofer, and H. Reinhardt, Phys. Rev. D **65**, 094008 (2002); C. S. Fischer and R. Alkofer, Phys. Lett. B **536**, 177 (2002).

[21] C. S. Fischer and R. Alkofer, Phys. Rev. D **67**, 094020 (2003).

[22] D. Zwanziger, Phys. Rev. D **65**, 094039 (2002).

[23] C. Lerche and L. von Smekal, Phys. Rev. D **65**, 125006 (2002).

[24] J. M. Pawlowski, D. F. Litim, S. Nedelko, and L. von Smekal, Phys. Rev. Lett. **93**, 152002 (2004); C. S.

Fischer and H. Gies, J. High Energy Phys. 10 (**2004**) 048.

[25] D. Zwanziger, Nucl. Phys. **B364**, 127 (1991).

[26] P. J. Silva and O. Oliveira, hep-lat/0511043.

[27] V. A. Miransky, Phys. Lett. **165B**, 401 (1985).

[28] W. J. Marciano and H. Pagels, Phys. Rep. **36**, 137 (1978).

[29] R. Alkofer, C. S. Fischer, and F. J. Llanes-Estrada, Phys. Lett. B **611**, 279 (2005).

[30] A. Hasenfratz, hep-lat/0511021.

[31] J. S. Ball and T. W. Chiu, Phys. Rev. D **22**, 2542 (1980).

[32] P. O. Bowman, U. M. Heller, D. B. Leinweber, M. B. Parappilly, A. G. Williams, and J. b. Zhang, Phys. Rev. D **71**, 054507 (2005).

[33] D. Zwanziger, Phys. Rev. D **67**, 105001 (2003).

[34] S. Capitani, M. Luscher, R. Sommer, and H. Wittig (ALPHA Collaboration), Nucl. Phys. **B544**, 669 (1999).

[35] V. Gimenez, V. Lubicz, F. Mescia, V. Porretti, and J. Reyes, Eur. Phys. J. C **41**, 535 (2005).

[36] J. Wennekers and H. Wittig, J. High Energy Phys. 09 (2005) 059.

[37] C. McNeile, Phys. Lett. B **619**, 124 (2005).

[38] D. Atkinson and D. W. Blatt, Nucl. Phys. **B151**, 342 (1979).

[39] G. Krein, C. D. Roberts, and A. G. Williams, Int. J. Mod. Phys. A **7**, 5607 (1992).

[40] C. J. Burden, C. D. Roberts, and A. G. Williams, Phys. Lett. B **285**, 347 (1992).

[41] P. Maris and H. A. Holties, Int. J. Mod. Phys. A **7**, 5369 (1992).

[42] R. Oehme, Int. J. Mod. Phys. A **10**, 1995 (1995).

[43] C. J. Burden, Phys. Rev. D **57**, 276 (1998); **59**, 037502 (1999).

[44] R. Alkofer, W. Detmold, C. S. Fischer, and P. Maris, Phys. Rev. D **70**, 014014 (2004).

[45] K. Osterwalder and R. Schrader, Commun. Math. Phys. **31**, 83 (1973); **42**, 281 (1975).

[46] U. Habel *et al.*, Z. Phys. A **336**, 423 (1990); **336**, 435 (1990); M. Stingl, Z. Phys. A **353**, 423 (1996).

[47] J. I. Skullerud, P. O. Bowman, A. Kizilersu, D. B. Leinweber, and A. G. Williams, J. High Energy Phys. 04 (2003) 047.

[48] M. S. Bhagwat, A. Holl, A. Krassnigg, C. D. Roberts, and P. C. Tandy, Phys. Rev. C **70**, 035205 (2004).

[49] M. S. Bhagwat and P. C. Tandy, Phys. Rev. D **70**, 094039 (2004).

[50] C. S. Fischer, F. Llanes-Estrada, and R. Alkofer, Nucl. Phys. B, Proc. Suppl. **141**, 128 (2005).

[51] A. Bender, C. D. Roberts, and L. Von Smekal, Phys. Lett. B **380**, 7 (1996).

[52] P. Maris, C. D. Roberts, and P. C. Tandy, Phys. Lett. B **420**, 267 (1998).

[53] S. Eidelman *et al.* (Particle Data Group Collaboration), Phys. Lett. B **592**, 1 (2004).